ChemPhysChem

Research Article
doi.org/10.1002/cphc.202200226

Chemistry Europe
European Chemical Societies Publishing

www.chemphyschem.org

The Hunter Falls Prey: Photoinduced Oxidation of C_{60} in Inclusion Complex with Perfluorocycloparaphenylene

Olga A. Stasyuk,[a, b] Anton J. Stasyuk,*[a, b] Miquel Solà,*[a] and Alexander A. Voityuk*[a]

Perfluorocycloparaphenylenes (PFCPPs) are cycloparaphenylenes (CPPs) in which all hydrogen atoms have been replaced by fluorine atoms. Like CPPs, PFCPPs are highly strained, hoop-shaped π-conjugated molecules. In this article, we report a computational modeling of photoinduced electron transfer processes in the inclusion complex of **PF[10]CPP** with C_{60} fullerene. Its unique feature is the favorable electron transfer from C_{60} to the host molecule. The photooxidation of C_{60} is predicted to occur on a sub-nanosecond timescale. The **PF-[10]CPP⊃C_{60}** dyad is the first nanoring-fullerene complex in which C_{60} acts as an electron donor in the photoinduced charge separation.

Introduction

The importance of converting sunlight into electricity and chemical fuels cannot be overstated. A lot of attention and efforts have been paid to design and prepare model compounds that mimic natural photosynthetic systems.[1] Generation of long-lived charge-separated (CS) states with a high quantum yield and a long distance between radical ions to prevent their recombination is of key essence for such donor-acceptor systems.[2] Since their discovery in 1985,[3] fullerenes have attracted considerable attention as efficient electron acceptors in photovoltaics due to their properties such as a narrow HOMO–LUMO gap and good electron transportability. However, there are several known disadvantages of fullerenes as a component of photovoltaic devices,[4] which can dramatically decrease the efficiency of photocurrent generation.[5] In particular, some restrictions in functional tuning at the molecular level and a tendency towards self-aggregation make it difficult to develop materials with desired properties. On the other hand, due to their chemical nature and spherical shape, fullerenes are an ideal guest molecule to form stable complexes with various macrocyclic host molecules[6] such as cyclodextrines,[7] calix[8]arenes[8] or cycloparaphenylenes[9] (CPP) because of the concave-convex complementarity. The formation of host-guest complexes effectively suppresses fullerene aggregation and thereby facilitates the conversion of light into electricity. The significant advances in CPP chemistry over the past decade have enabled the synthesis of CPPs with the diameter from 7 to 28 Å, that are suitable hosts for many fullerenes.[9d,10] A number of supramolecular donor-acceptor (DA) complexes of CPP with various fullerenes including endohedral species have been reported to be capable of photoinduced electron transfer (PET).[11] In such complexes, CPPs act as an electron donor.

Recently, Itami et al. reported the synthesis and X-ray characterization of perfluorocycloparaphenylenes (PFCPPs) of different sizes, which form a new class of ring-shaped perfluoroarenes.[12] PFCPPs are CPPs, in which all hydrogen atoms are replaced by fluorine atoms. This substitution strongly influences electronic properties of CPPs. Suitable size of ring cavity and increase in electron affinity through perfluorination of CPP encouraged us to investigate **PF[10]CPP** in combination with C_{60}. Electronic and photoinduced electron transfer properties of **PF[10]CPP⊃C_{60}** host-guest complex were investigated using time-dependent density-functional theory (TD-DFT) and compared with those of the well-studied **[10]CPP⊃C_{60}** complex. Our results clearly demonstrate that **PF[10]CPP⊃C_{60}** has unique PET properties. In the complex, **PF[10]CPP** acts as a strong electron acceptor while C_{60} is an electron donor, in contrast to what was previously observed in nanoring-fullerene dyads.

Computational Details

Geometry optimizations were performed employing BLYP exchange – correlation functional,[13] Ahlrichs' def2-SVP basis set,[14] and the resolution of identity approximation[15] as implemented in the program ORCA 4.1.2.[16] The formation energy of the complexes as well as their strain energies were computed with the BLYP/def2-TZVP//BLYP/def2-SVP scheme.[17] The canonical energy decomposition analysis (EDA) was performed using the Amsterdam Density Functional (ADF) program.[18] Electronic structure calculations and vertical excitation energies were calculated using the Tamm-Dancoff approximation (TDA),[19] the range-separated functional CAM-B3LYP,[20] the def2-SVP basis set,[14] and the program Gaussian 16 (rev. A03).[21] Recently, some of us have benchmarked different

[a] Dr. O. A. Stasyuk, Dr. A. J. Stasyuk, Prof. Dr. M. Solà, Prof. Dr. A. A. Voityuk
Institut de Química Computacional i Catàlisi and Departament de Química, Universitat de Girona
C/ Maria Aurèlia Capmany 69, 17003 Girona, Spain
E-mail: antony.stasuk@gmail.com
miquel.sola@udg.edu
alexander.voityuk@gmail.com
[b] Dr. O. A. Stasyuk, Dr. A. J. Stasyuk
Faculty of Chemistry, University of Warsaw
Pasteura 1, 02-093 Warsaw, Poland

Supporting information for this article is available on the WWW under https://doi.org/10.1002/cphc.202200226

density functional approximations and showed that CAM-B3LYP functional is the best choice for evaluation of charge-transfer rates in fullerene-based materials.[22] The empirical dispersion D3 correction was computed using the Becke-Johnson damping scheme.[23] The population analysis and calculation of Hirshfeld[24] and CM5[25] charges were carried out with the Gaussian 16 program. The topological analysis of the electron density distribution was conducted using the "Quantum Theory of Atoms in Molecules" (QTAIM).[26] The AIMALL suite of programs[27] was applied to evaluate the bond critical point properties and associated bond descriptors. To visualize molecular structures and frontier molecular orbitals, the program Chemcraft 1.8 was used.[28] Details on the analysis of excited states, calculation solvent effects, electron transfer rates, reorganization and interaction energies can be found in the Supporting Information.

Results and Discussion

Structure and Ground State Properties

First, we compared the electronic properties of **PF[10]CPP** and **[10]CPP**, and their binary complexes with C_{60} (Figure 1). As seen in Figure 1, HOMO and LUMO energies of **PF[10]CPP** and **[10]CPP** nanorings differ significantly. Replacing hydrogen atoms with fluorine atoms lowers the HOMO energy by more than 2 eV, while the LUMO energy decreases by about 1 eV. In the complexes, a significant difference in the electronic properties is observed despite their structural similarity. The HOMO of **[10]CPP⊃C_{60}** is localized on the host unit, while the HOMO of **PF[10]CPP⊃C_{60}** is localized on C_{60}. In both complexes, LUMO is localized on C_{60}. The formation of complexes has a rather weak effect on the HOMO and LUMO energies of the individual fragments. In particular, HOMO energies remain almost unchanged (within 0.1 eV). A shift in the LUMOs does not exceed 0.3 eV (Figure 1). These small differences in orbital energies by passing from the individual fragments to the dyads indicate the lack of charge separation in the ground state (GS). Also, the population analysis does not reveal any significant charge transfer between the host and guest molecules in both systems (Table S1 in SI).

To estimate the stability of the complexes, the interaction energy (ΔE_{int}) between the nanorings and fullerene was computed. For **PF[10]CPP⊃C_{60}** and **[10]CPP⊃C_{60}** systems, ΔE_{int} was found to be −47.7 and −56.8 kcal/mol. It can be assumed that **PF[10]CPP⊃C_{60}** complex is formed in solution, since fullerene complexes with a noticeably lower interaction energy are known. For example, ΔE_{int} for the complex of C_{60} with π-extended corannulene bowl is only −31 kcal/mol,[29a] but the existence of such a complex in solution has been established experimentally.[29b] The dispersion interactions play a major role in the stability of the complex, as shown earlier for systems of a similar nature.[11c,30] To get more insight, we performed the energy decomposition analysis (EDA) of the interaction energy using a Morokuma-type method.[31] Within this scheme, the interaction energy is divided into four components: Pauli repulsion (ΔE_{Pauli}), electrostatic (ΔE_{elstat}), orbital interaction (ΔE_{oi}), and dispersion (ΔE_{disp}) terms (see computational details in SI). The EDA results are merged in Table 1. The destabilizing term (Pauli repulsion) for **PF[10]CPP⊃C_{60}** is significantly larger than for **[10]CPP⊃C_{60}** (131.1 kcal/mol vs. 82.1 kcal/mol). Among the intermolecular attraction (electrostatic, orbital, and dispersion interactions), the dispersion term dominates and amounts to 54 and 62%, while the electrostatic term is 32 and 25% for **PF[10]CPP⊃C_{60}** and **[10]CPP⊃C_{60}**, respectively. The orbital interactions term is similar (14 and 12%).

To explain the noticeable difference in the Pauli repulsion, we compared the geometrical structures of the complexes. The

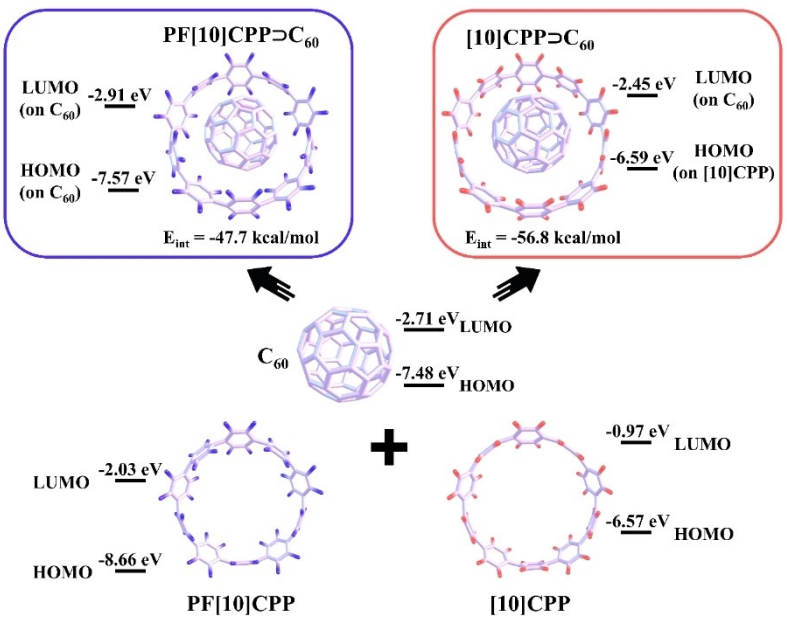

Figure 1. HOMO and LUMO energies of **PF[10]CPP⊃C_{60}** and **[10]CPP⊃C_{60}** and their subunits.

Table 1. EDA results for **PF[10]CPP⊃C_{60}** and **[10]CPP⊃C_{60}** complexes.[a]

Complex	Energy terms, [kcal/mol]				
	ΔE_{Pauli}	ΔE_{elstat}	ΔE_{oi}	ΔE_{disp}	ΔE_{int}
[10]CPP⊃C_{60}	82.07	−35.20 (25.3%)	−17.25 (12.4%)	−86.46 (62.3%)	−56.84
PF[10]CPP⊃C_{60}	131.08	−56.28 (31.5%)	−25.32 (14.1%)	−97.20 (54.4%)	−47.73

[a] The percentage contributions to the sum of attraction energies ($\Delta E_{elstat} + \Delta E_{oi} + \Delta E_{disp}$) are given in parentheses.

guest molecule in both complexes is the same (**C_{60}**). Its effective radius, i.e. mean distance from center to each carbon atom, $R_{eff} = 5.15$ Å. Thus, we focused our attention on the hosts, **PF[10]CPP** and **[10]CPP**. The most stable structure of the nanorings corresponds to an alternating zigzag orientation of phenylene units. The radii for **PF[10]CPP** and **[10]CPP** are equal to 6.86 and 6.89 Å, respectively. The formation of the complexes insignificantly affects their size; the radius of **PF[10]CPP** increases from 6.86 to 6.90 Å, while the radius of **[10]CPP** decreases from 6.89 to 6.87 Å (Figures S1 and S2 in SI). Also, there are some changes in the twist angle between phenyl rings. For **[10]CPP**, they do not exceed 1.5° (the angles change from 30° to 28.5–29°). In the free **PF[10]CPP**, the twist angle is equal to 53°, it decreases to 47° due to the inclusion of **C_{60}** which leads to a deformed structure of the host. In turn, a noticeable difference in the distance between fullerene and hydrogen/fluorine atoms is observed by increasing the twist angles. For example, the difference for close and distant hydrogen/fluorine atoms in **[10]CPP⊃C_{60}** is about 1.2 Å, while for **PF[10]CPP⊃C_{60}** it becomes 2 Å (Figure S3 in SI). The strain energy of the considered nanorings was estimated using a homodesmotic reaction proposed by Itami and co-workers.[32] The strain energies in **[10]CPP** and **[10]CPP⊃C_{60}** are 52.8 and 53.4 kcal/mol, respectively. For **PF[10]CPP**, the strain energy changes from 54.9 to 57.5 kcal/mol (Table S1 in SI). Thus, the weaker intermolecular interactions in **PF[10]CPP⊃C_{60}** compared to those in **[10]CPP⊃C_{60}** can be explained by stronger host-guest repulsion (see ΔE_{Pauli} in Table 1) caused by the change of H by F atoms, the latter with three more electron pairs in the **PF[10]CPP** fragment.

A topological analysis based on the QTAIM theory was used to obtain additional information about the host-guest interaction in the complexes. The electron density, its Laplacian, and other topological parameters at bond critical points (BCPs) were calculated (see Table S2). The analysis confirmed that the interactions between fragments in the **PF[10]CPP⊃C_{60}** and **[10]CPP⊃C_{60}** complexes correspond mostly to π···π interactions. **PF[10]CPP⊃C_{60}** is characterized by a larger number of BCPs as compared to **[10]CPP⊃C_{60}** (20 *vs.* 17). In **[10]CPP⊃C_{60}**, BCPs were found only between carbon atoms of subunits. However, in **PF[10]CPP⊃C_{60}**, BCPs were additionally detected between fluorine atoms and carbon atoms of fullerene, which is associate with different twist angles between phenyl rings in the complexes. The descriptors of BCPs indicate that the π···π interaction between fragments in **[10]CPP⊃C_{60}** is stronger than in **PF[10]CPP⊃C_{60}**. The characteristics of BCPs for C···C and F···C interactions in **PF[10]CPP⊃C_{60}** are similar. The QTAIM molecular graphs for **PF[10]CPP⊃C_{60}** and **[10]CPP⊃C_{60}** are given in Figure S4, SI. The topology of the host-guest interactions in the complexes was also described using non-covalent interaction index (NCI).[33] The shape of NCI isosurfaces clearly demonstrates the difference between the intermolecular interactions in **PF[10]CPP⊃C_{60}** and **[10]CPP⊃C_{60}**. In the case of **[10]CPP⊃C_{60}**, the isosurface is fairly uniform between **C_{60}** and **[10]CPP**, while for **PF[10]CPP⊃C_{60}** it has a wavy character with maxima in the region of closely spaced fluorine atoms. The reduced density gradient (RDG) plots and NCI isosurfaces are presented in Figures S5 and S6, SI.

Singlet Excited States

The significant differences in HOMOs and LUMOs described above for the **PF[10]CPP⊃C_{60}** and **[10]CPP⊃C_{60}** complexes suggest that PET properties of the complexes should also be different. The contributions of the guest and host molecules to the electronic density of the lowest 80 excited states were analyzed for each complex. Three types of excited states were identified: (1) locally excited (LE) states, where exciton is mostly localized either on the guest (LE^{Guest}) or on the host molecule (LE^{Host}) and charge transfer is smaller than 0.1 ***e*** ($CT < 0.1$ ***e***); (2) charge transfer (CT) states showing significant charge separation ($CT > 0.8$ **e**); and (3) mixed states, where both LE and CT states contribute substantially (0.1 ***e*** $< CT < 0.8$ ***e***).

In the gas phase, the 80 lowest vertical singlet excitation energies of **[10]CPP⊃C_{60}** range from 2.51 to 4.54 eV. The lowest-lying excited state at 2.51 eV is LE^{Guest} state, which is associated with a HOMO-3→LUMO+2 transition (Table 2). The lowest LE^{Host} state localized on **[10]CPP** was found at 3.43 eV (1 eV higher in energy compared to LE^{Guest}) and relates to a HOMO→LUMO+6 transition. Among the studied excited states only one type of CT was found: **[10]CPP$^+$⊃C_{60}^-**, generated by electron transfer from **[10]CPP** to **C_{60}**. This CT state associated with a HOMO→LUMO transition is characterized by $CT = 0.99$ ***e*** and lies about 0.2 eV higher than the first excited state.

The 80 lowest-lying vertical singlet excited states of **PF-[10]CPP⊃C_{60}** are located between 2.49 eV and 4.53 eV. The energy of the LE^{Guest} states in both complexes is almost identical. However, the energy of the LE^{Host} in **PF[10]CPP⊃C_{60}**, 4.06 eV, is significantly higher than in **[10]CPP⊃C_{60}**. In this complex, two types of CT states were found. The first state, **PF[10]CPP$^+$⊃C_{60}^-** (CT1), is similar to that in **[10]CPP⊃C_{60}**, while the other CT state, **PF[10]CPP$^-$⊃C_{60}^+** (CT2), is generated by electron transfer from **C_{60}** to **PF[10]CPP**. Important to note that the energy of CT2 state is about 0.3 eV lower than the energy of CT1. Figures S7 and S8 in SI show natural transition orbitals that represent the lowest LE and CT states in the complexes.

Effects of Environment and Electron Transfer Rates

A well-proven COSMO-like model[34] with dichloromethane (DCM) as the solvent was applied to estimate the effect of polar

Table 2. Excitation energies (E_x, eV), main singly excited configuration (HOMO(H)–LUMO(L)) and its weight (W), oscillator strength (f), extent of charge transfer (CT, e) or localization of exciton (X) computed for **PF[10]CPP⊃C_{60}** and **[10]CPP⊃C_{60}** complexes in the gas-phase (VAC) and dichloromethane (DCM).

	Supramolecular host-guest systems			
	[10]CPP⊃C_{60}		**PF[10]CPP⊃C_{60}**	
	VAC	DCM	VAC	DCM
	LE^{Guest} (**C_{60}**)			
E_x	2.508	2.501	2.486	2.476
Transition (W)	H-3−L+2 (0.63)	H-3−L+2 (0.27)	H-4−L (0.84)	H−L (0.76)
f	<0.001	<0.001	<0.001	<0.001
X	0.952	0.948	0.937	0.936
	LE^{Host} (**[10]CPP/PF[10]CPP**)			
E_x	3.428	3.433	4.056	4.057
Transition (W)	H−L+6 (0.30)	H-4−L+5 (0.09)	H-5−L+3 (0.49)	H-5−L+3 (0.50)
f	<0.001	<0.001	<0.001	<0.001
X	0.939	0.938	0.905	0.906
	Most absorptive (MA) transition[a]			
E_x	3.817	3.823	4.462	4.430
Transition (W)	H−L+7 (0.23)	H−L+7 (0.28)	H-5−L+4 (0.15)	H-5−L+4 (0.19)
f	1.303	2.624	0.647	1.444
Localization	**[10]CPP**	**[10]CPP**	**PF[10]CPP**	**PF[10]CPP**
CT	0.237	0.081	0.217	0.250
	CT1 (**[10]CPP/PF[10]CPP→C_{60}**)			
E_x	2.736	2.519	4.138	3.880
Transition (W)	H−L (0.96)	H−L (0.96)	H-5−L (0.70)	H-5−L (0.92)
f	0.008	0.001	<0.001	<0.001
CT	0.982	0.983	0.855	0.946
	CT2 (**C_{60}→[10]CPP/PF[10]CPP**)			
E_x	n/f[b]		3.818	3.781
Transition (W)			H-4−L+3 (0.76)	H−L+3 (0.67)
f			<0.001	<0.001
CT				0.803

[a] mixed states with significant contributions of LE and CT; [b] states of interest are not found within 80 lowest excited states.

environment on electronic excitations. The GS solvation energy of **PF[10]CPP⊃C_{60}** and **[10]CPP⊃C_{60}** complexes is equal to −0.44 and −0.40 eV, respectively. The dipole moment is 0.04 and 0.01 D, respectively. It is well known that the solvation energy of LE states is quite similar to that of the ground state, but it is usually much stronger for CT states. The changes in the dipole moment, when going from GS to LE states, are quite small (~0.1 D), and, as expected, the computed solvation energies of the GS and LE states are very similar. Considering the high symmetry of the studied complexes leading to efficient charge delocalization, it can be assumed that the solvation energy of the CT states is not much higher than that of the GS. Besides, the difference in the dipole moment of CT and GS states is small and does not exceed 0.04 and 0.20 D for **PF[10]CPP⊃C_{60}** and **[10]CPP⊃C_{60}** complexes, respectively. Consequently, the solvation energy of the CT1 state is only −0.70 eV for **PF[10]CPP⊃C_{60}** and −0.62 eV for **10]CPP⊃C_{60}**. The solvation energy of the CT2 state of **PF[10]CPP⊃C_{60}** is −0.48 eV. The stronger solvent stabilization of the CT1 state compared to the CT2 is due to the different CT values. Indeed, the CT1 state is characterized by almost complete charge transfer (CT = 0.95 ***e***), while in the CT2 only 0.80 ***e*** is transferred. Figure 2 displays the energies of the GS, LE, and CT states in the gas phase and DCM. The changes in the dipole moment and solvation energies for all considered excited states are given in Table S3.

For both systems, the CT states are characterized by a very weak oscillator strength and, therefore, cannot be directly populated by light absorption. However, they can be generated by a decay of the lowest LE states. For the **PF[10]CPP⊃C_{60}** and **[10]CPP⊃C_{60}** complexes, most absorptive transitions are localized on the host unit. The MA states extremely fast decay by internal conversion to the lowest LE^{Host}. Thus, charge separation process was considered between LE^{Host} and CT state of interest. The rates of charge separation (k_{CS}) and charge recombination (k_{CR}) were calculated using the semi-classical method by Ulstrup and Jortner.[35] Within this approach, the intramolecular relaxation associated with ET is described by an effective vibrational mode, and the rate is controlled by four parameters: electronic coupling of the initial and final states V_{ij}, solvation reorganization energy λ_s, reaction Gibbs energy ΔG^0, and effective Huang-Rhys factor S_{eff}. The computed parameters and rates in DCM are listed in Table 3. The rates were estimated using the effective frequency of 1600 cm^{-1}, which corresponds to the stretching of C=C bonds. Note that the calculated rates of charge separation do not change significantly by varying the effective frequency from 1400 to 1800 cm^{-1}.[30,36] For **PF[10]CPP⊃C_{60}**, we additionally checked the influence of the frequency choice on the estimated ET rate (Table S4, SI) and found it to be insignificant.

The charge separation in **[10]CPP⊃C_{60}** is characterized by a large negative Gibbs energy value. This reaction takes place in the inverted Marcus region ($|\Delta G^0| > \lambda$) and the estimated CS

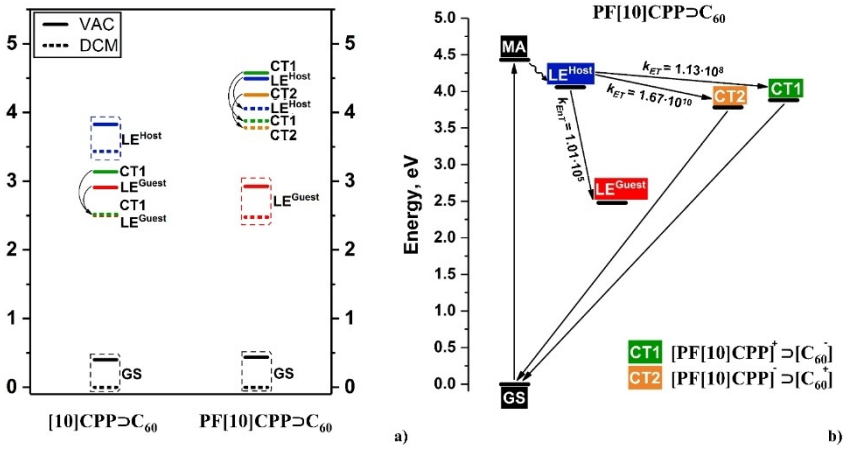

Figure 2. (a) Energies of LE and CT states (in eV) computed for **PF[10]CPP⊃C$_{60}$** and **[10]CPP⊃C$_{60}$** complexes in vacuum (VAC) and dichloromethane (DCM); (b) Energy levels and ET rates for **PF[10]CPP⊃C$_{60}$** in DCM.

Table 3. Gibbs energy ΔG^0 (in eV), electronic coupling V_{ij} (in eV), solvent (λ_s) and internal (λ_i) reorganization energy (in eV), Huang-Rhys factor (S_{eff}) and rates k_X (in s^{-1}) for CS and CR processes computed for **PF[10]CPP⊃C$_{60}$** and **[10]CPP⊃C$_{60}$** complexes in DCM.

Complex	Transition	$\Delta G^{0[a]}$, eV	$\lvert V_{ij} \rvert$, eV	Reorg. energy, eV λ_i	λ_s	S_{eff}[b]	k_X, s^{-1}
[10]CPP⊃C$_{60}$	$LE^{Host}\rightarrow CT1$	−0.914	$1.66\cdot10^{-4}$	0.158	0.181	0.796	$2.20\cdot10^{7}$
	$CT1\rightarrow GS$	−2.519	$4.12\cdot10^{-3}$	0.134	0.181	0.675	$3.90\cdot10^{1}$
PF[10]CPP⊃C$_{60}$	$LE^{Host}\rightarrow LE^{Guest}$	−0.052	$2.05\cdot10^{-6}$	0.184	0.009	0.932	$1.01\cdot10^{5}$
	$LE^{Host}\rightarrow CT1$	−0.177	$6.70\cdot10^{-5}$	0.125	0.081	0.630	$1.13\cdot10^{8}$
	$LE^{Host}\rightarrow CT2$	−0.276	$8.84\cdot10^{-4}$	0.185	0.096	0.933	$1.67\cdot10^{10}$
	$CT1\rightarrow GS$	−3.880	$2.01\cdot10^{-4}$	0.114	0.081	0.575	$[2.85\cdot10^{-13}]$
	$CT2\rightarrow GS$	−3.781	$3.99\cdot10^{-5}$	0.196	0.096	0.988	$[1.18\cdot10^{-9}]$

[a] Gibbs energy difference between the given states. [b] Effective value of the Huang-Rhys factor $S_{eff}=\lambda_i/\hbar\omega_{eff}$, where $\hbar\omega_{eff}$ is set to 1600 cm^{-1}.

rate is quite low ($2.2\cdot10^7$ s^{-1}). The electron transfer in **PF[10]CPP⊃C$_{60}$** complex occurs in the normal Marcus regime ($|\Delta G^0| < \lambda$) and is fast. Note that PET, in which **C$_{60}$** fullerene acts as electron donor generating **PF[10]CPP$^-$⊃C$_{60}^+$** (CT2), is by two orders of magnitude faster than the formation of **PF[10]CPP$^+$⊃C$_{60}^-$** (CT1, **C$_{60}$** is electron acceptor). The charge recombination reactions take place in a deep inverted Marcus region, and their rates are dramatically lower compared to the charge separation rates, although the rates determined in the deep inverted Marcus region are not reliable. To get more insight, we additionally considered exciton transfer between LE^{Host} and LE^{Guest} states in **PF[10]CPP⊃C$_{60}$**,. The reorganization energy for exciton transfer is relatively small (Table 3). Thus, the rate of this process determined by the Franck-Condon factor will be maximum at relatively small negative values of the Gibbs energy. The fastest rate for the exciton transfer between the fragments was found to be equal to $1.0\cdot10^5$ s^{-1}, when the difference in energy between LE states is −0.052 eV. As seen, the exciton transfer process is much slower than the related charge separation reaction and, thus, cannot compete with ET.

Since the electron transfer in the **PF[10]CPP⊃C$_{60}$** complex is characterized by a rather small negative ΔG^0 (Table 3), the charge recombination CT1/CT2→LE^{Host} state can be considered as an alternative deactivation channel of the CT state. As seen in Table S5, the back electron transfer in **PF[10]CPP⊃C$_{60}$** complexes is significantly slower than charge separation. Thus, we can be sure that back electron transfer will not compete with generation of CT state.

Conclusions

In this work, we have studied the ground and excited-state properties of the complex formed by the fully fluorinated carbon nanoring and **C$_{60}$** fullerene. The low LUMO of **PF[10]CPP** and its ability to delocalize an excess electron make this nanoring an efficient electron acceptor. In the **PF[10]CPP⊃C$_{60}$** complex, we found an unusual photoinduced electron transfer from **C$_{60}$** to **PF[10]CPP**. This seems to be the first example of photooxidation of **C$_{60}$** in DA complexes with carbon nanohoops.

Author Contributions

O. A. S. Investigation, Formal analysis, Writing – original draft, Writing – review & editing; A. J. S. Investigation, Formal analysis, Writing – original draft, Writing – review & editing; M. S. Supervision, Writing – review & editing, Funding acquisition; A. A. V. Supervision, Writing – review & editing.

Acknowledgements

We are grateful for financial support from the Spanish MINECO (Network RED2018-102815-T, project PID2020-113711GB-I00, and Juan de la Cierva contract IJC2019-039846-I to A. J. S.), the Catalan DIUE (2017SGR39), and the University of Girona (POST-DOC-UdG 2021/31 to O. A. S.). This research was supported in part by PLGrid Infrastructure.

Conflict of Interest

The authors declare no conflict of interest.

Data Availability Statement

The data that support the findings of this study are available in the supplementary material of this article.

Keywords: computational chemistry · nanostructure · fullerene · electron transfer · donor-acceptor complex

[1] a) M. R. Wasielewski, *Chem. Rev.* **1992**, *92*, 435–461; b) R. L. House, N. Y. M. Iha, R. L. Coppo, L. Alibabaei, B. D. Sherman, P. Kang, M. K. Brennaman, P. G. Hoertz, T. J. Meyer, *J. Photochem. Photobiol. C* **2015**, *25*, 32–45.
[2] a) F. D'Souza, O. Ito, *Chem. Soc. Rev.* **2012**, *41*, 86–96; b) S. Fukuzumi, K. Ohkubo, T. Suenobu, *Acc. Chem. Res.* **2014**, *47*, 1455–1464.
[3] H. W. Kroto, J. R. Heath, S. C. O'Brien, R. F. Curl, R. E. Smalley, *Nature* **1985**, *318*, 162–163.
[4] a) B. M. Illescas, N. Martín, *C. R. Chim.* **2006**, *9*, 1038–1050; b) Y. He, Y. Li, *Phys. Chem. Chem. Phys.* **2011**, *13*, 1970–1983; c) T. Liu, A. Troisi, *Adv. Mater.* **2013**, *25*, 1038–1041.
[5] a) B. C. Thompson, J. M. J. Fréchet, *Angew. Chem. Int. Ed.* **2008**, *47*, 58–77; *Angew. Chem.* **2008**, *120*, 62–82; b) L.-M. Chen, Z. Hong, G. Li, Y. Yang, *Adv. Mater.* **2009**, *21*, 1434–1449; c) H. Kang, W. Lee, J. Oh, T. Kim, C. Lee, B. J. Kim, *Acc. Chem. Res.* **2016**, *49*, 2424–2434.
[6] Q. Shi, X. Wang, B. Liu, P. Qiao, J. Li, L. Wang, *Chem. Commun.* **2021**, *57*, 12379–12405.
[7] Q.-D. Hu, G.-P. Tang, P. K. Chu, *Acc. Chem. Res.* **2014**, *47*, 2017–2025.
[8] C. Redshaw, *Coord. Chem. Rev.* **2003**, *244*, 45–70.
[9] a) T. Kawase, H. Kurata, *Chem. Rev.* **2006**, *106*, 5250–5273; b) T. Iwamoto, Y. Watanabe, T. Sadahiro, T. Haino, S. Yamago, *Angew. Chem. Int. Ed.* **2011**, *50*, 8342–8344; *Angew. Chem.* **2011**, *123*, 8492–8494; c) J. Xia, J. W. Bacon, R. Jasti, *Chem. Sci.* **2012**, *3*, 3018–3021; d) M. Hermann, D. Wassy, B. Esser, *Angew. Chem. Int. Ed.* **2021**, *60*, 15743–15766; *Angew. Chem.* **2021**, *133*, 15877–15900.
[10] S. E. Lewis, *Chem. Soc. Rev.* **2015**, *44*, 2221–2304.
[11] a) D. Lu, Q. Huang, S. Wang, J. Wang, P. Huang, P. Du, *Front. Chem.* **2019**, *7*, 668; b) Y. Xu, M. von Delius, *Angew. Chem. Int. Ed.* **2020**, *59*, 559–573; *Angew. Chem.* **2020**, *132*, 567–582; c) O. A. Stasyuk, A. J. Stasyuk, M. Solà, A. A. Voityuk, *Chem. Eur. J.* **2021**, *27*, 8737–8744; d) S. Hitosugi, K. Ohkubo, R. Iizuka, Y. Kawashima, K. Nakamura, S. Sato, H. Kono, S. Fukuzumi, H. Isobe, *Org. Lett.* **2014**, *16*, 3352–3355.
[12] H. S. K. Itami, H. Shudo, M. Kuwayama, M. Shimasaki, T. Nishihara, Y. Takeda, T. Kuwabara, A. Yagi, Y. Segawa, *ChemRxiv*, preprint, **2021**, DOI: 10.33774/chemrxiv-2021-7kd63.
[13] a) A. D. Becke, *Phys. Rev. A* **1988**, *38*, 3098–3100; b) C. Lee, W. Yang, R. G. Parr, *Phys. Rev. B* **1988**, *37*, 785–789.
[14] a) F. Weigend, R. Ahlrichs, *Phys. Chem. Chem. Phys.* **2005**, *7*, 3297–3305; b) F. Weigend, *Phys. Chem. Chem. Phys.* **2006**, *8*, 1057–1065.
[15] a) K. Eichkorn, O. Treutler, H. Öhm, M. Häser, R. Ahlrichs, *Chem. Phys. Lett.* **1995**, *240*, 283–290; b) K. Eichkorn, F. Weigend, O. Treutler, R. Ahlrichs, *Theor. Chem. Acc.* **1997**, *97*, 119–124.
[16] F. Neese, *WIREs Comput. Mol. Sci.* **2018**, *8*, e1327.
[17] F. Weigend, M. Häser, H. Patzelt, R. Ahlrichs, *Chem. Phys. Lett.* **1998**, *294*, 143–152.
[18] a) ADF 2019, Theoretical Chemistry, Vrije Universiteit, Amsterdam, The Netherlands, http://www.scm.com; b) G. te Velde, F. M. Bickelhaupt, E. J. Baerends, C. Fonseca Guerra, S. J. A. van Gisbergen, J. G. Snijders, T. Ziegler, *J. Comput. Chem.* **2001**, *22*, 931–967.
[19] S. Hirata, M. Head-Gordon, *Chem. Phys. Lett.* **1999**, *314*, 291–299.
[20] T. Yanai, D. P. Tew, N. C. Handy, *Chem. Phys. Lett.* **2004**, *393*, 51–57.
[21] M. J. Frisch, G. W. Trucks, H. B. Schlegel, G. E. Scuseria, M. A. Robb, J. R. Cheeseman, G. Scalmani, V. Barone, G. A. Petersson, H. Nakatsuji, X. Li, M. Caricato, A. V. Marenich, J. Bloino, B. G. Janesko, R. Gomperts, B. Mennucci, H. P. Hratchian, J. V. Ortiz, A. F. Izmaylov, J. L. Sonnenberg, Williams, F. Ding, F. Lipparini, F. Egidi, J. Goings, B. Peng, A. Petrone, T. Henderson, D. Ranasinghe, V. G. Zakrzewski, J. Gao, N. Rega, G. Zheng, W. Liang, M. Hada, M. Ehara, K. Toyota, R. Fukuda, J. Hasegawa, M. Ishida, T. Nakajima, Y. Honda, O. Kitao, H. Nakai, T. Vreven, K. Throssell, J. A. Montgomery Jr., J. E. Peralta, F. Ogliaro, M. J. Bearpark, J. J. Heyd, E. N. Brothers, K. N. Kudin, V. N. Staroverov, T. A. Keith, R. Kobayashi, J. Normand, K. Raghavachari, A. P. Rendell, J. C. Burant, S. S. Iyengar, J. Tomasi, M. Cossi, J. M. Millam, M. Klene, C. Adamo, R. Cammi, J. W. Ochterski, R. L. Martin, K. Morokuma, O. Farkas, J. B. Foresman, D. J. Fox, *Gaussian 16*, revision C.01; Gaussian, Inc.: Wallingford, CT, **2016**.
[22] P. Besalú-Sala, A. A. Voityuk, J. M. Luis, M. Solà, *Phys. Chem. Chem. Phys.* **2021**, *23*, 5376–5384.
[23] a) S. Grimme, J. Antony, S. Ehrlich, H. Krieg, *J. Chem. Phys.* **2010**, *132*, 154104; b) S. Grimme, S. Ehrlich, L. Goerigk, *J. Comput. Chem.* **2011**, *32*, 1456–1465.
[24] F. L. Hirshfeld, *Theor. Chim. Acta* **1977**, *44*, 129–138.
[25] A. V. Marenich, S. V. Jerome, C. J. Cramer, D. G. Truhlar, *J. Chem. Theory Comput.* **2012**, *8*, 527–541.
[26] R. F. W. Bader, *Chem. Rev.* **1991**, *91*, 893–928.
[27] *T.A.K. AIMAll (Version 14.06.21)*, TK Gristmill Software, Overland Park KS, USA, **2019** (aim.tkgristmill.com).
[28] *Chemcraft – graphical software for visualization of quantum chemistry computations.* https://www.chemcraftprog.com.
[29] a) O. A. Stasyuk, A. J. Stasyuk, M. Solà, A. A. Voityuk, *Nanoscale Adv.* **2022**, *4*, 2180–2188; b) H. Yokoi, Y. Hiraoka, S. Hiroto, D. Sakumaki, S. Seki, S. Shinokubo, *Nat. Commun.* **2015**, *6*, 8215.
[30] A. J. Stasyuk, O. A. Stasyuk, M. Solà, A. A. Voityuk, *Chem. Commun.* **2020**, *56*, 12624–12627.
[31] a) K. Morokuma, *J. Chem. Phys.* **1971**, *55*, 1236–1244; b) F. M. Bickelhaupt, E. J. Baerends, in *Reviews in Computational Chemistry*, vol. 15 (Eds.: K. B. Lipkowitz, D. B. Boyd), John Wiley & Sons, Inc., **2000**, pp. 1–86.
[32] Y. Segawa, H. Omachi, K. Itami, *Org. Lett.* **2010**, *12*, 2262–2265.
[33] E. R. Johnson, S. Keinan, P. Mori-Sánchez, J. Contreras-García, A. J. Cohen, W. Yang, *J. Am. Chem. Soc.* **2010**, *132*, 6498–6506.
[34] a) A. Klamt, *J. Phys. Chem.* **1996**, *100*, 3349–3353; b) A. J. Stasyuk, O. A. Stasyuk, M. Solà, A. A. Voityuk, *Phys. Chem. Chem. Phys.* **2019**, *21*, 25098–25107; c) A. J. Stasyuk, O. A. Stasyuk, M. Solà, A. A. Voityuk, *J. Phys. Chem. B* **2020**, *124*, 9095–9102.
[35] J. Ulstrup, J. Jortner, *J. Chem. Phys.* **1975**, *63*, 4358–4368.
[36] O. A. Stasyuk, A. J. Stasyuk, M. Solà, A. A. Voityuk, *Phys. Chem. Chem. Phys.* **2021**, *23*, 2126–2133.

Manuscript received: April 5, 2022
Revised manuscript received: May 13, 2022
Accepted manuscript online: May 19, 2022
Version of record online: June 17, 2022